Received 9 February 2017; revised 7 July 2017; accepted 19 July 2017. Date of publication 1 August 2017;
date of current version 23 August 2017. The review of this paper was arranged by Editor S. Chakrabarti.

Digital Object Identifier 10.1109/JEDS.2017.2731119

Nonlinear Thermoelectroelastic Analysis of III-N Semiconductor Devices

M. G. ANCONA (Member, IEEE)

Electronic Science and Technology Division, Naval Research Laboratory, Washington, DC 20375, USA

CORRESPONDING AUTHOR: M. G. ANCONA (e-mail: ancona@estd.nrl.navy.mil)

ABSTRACT The diffusion-drift electron transport description is combined with finite deformation theory to model thermoelectroelastic behaviors in piezoelectric semiconductors under conditions when the mechanical strains/displacements are not small so that the usual assumption of linearity cannot be justified. The nonlinear treatment includes both kinematic and constitutive corrections as well as a proper treatment of the electrostatic conditions at free surfaces. The theory is illustrated using numerical simulations of various III-N devices of technological interest, including of conventional AlGaN/GaN HEMTs and of semiconducting microelectromechanical structures that can require the nonlinear theory's rotational invariance even when the strains are small. Despite uncertainties in the values of the various material coefficients, it seems likely that the nonlinear corrections are often substantial.

INDEX TERMS Drift-diffusion, finite deformation, gallium nitride, nonlinear theory, piezoelectric semiconductors.

I. INTRODUCTION

Piezoelectric semiconductors such as CdS and ZnO have received attention for many decades with the older literature primarily concerned with wave phenomena and acoustoelectric interactions [1], while later work has emphasized lower frequency behavior and devices [2], including in the area that has been called "piezotronics" [3], [4]. For the continuum modeling of such devices, almost all work to date has utilized an amalgam of the linear theory of piezoelectricity and diffusion-drift electron transport theory. Because of their recent technological prominence, the III-N materials (i.e., GaN, AlN, InN, and their alloys) have been a main focus of electromechanical modeling [5], with one study by the present author being on the characteristics and reliability of GaN HEMTs with coupling to heat generation/conduction included [6]. An important potential limitation of most (though not all [7]) such simulations is an underlying and often implicit assumption that the mechanical deformations are "small" so that the governing equations linearize and reduce to the usual equations. The goal of this paper is to discuss in systematic fashion the general nonlinear continuum theory that is needed when this assumption is not justified, and to illustrate it with technologically relevant examples involving the III-N materials.

It has long been recognized that in the presence of *finite* (*i.e.*, not necessarily "small") mechanical deformation, a linearized description is not valid, higher order terms must be considered, and it becomes imperative that the entire theory be carefully reformulated in a manner consistent with basic principles of classical field theory [8], [9]. How to do this for elasticity was a landmark achievement of Cauchy early in the 19th century, but its proper formulation for situations involving electromechanical coupling such as piezoelectricity was not understood until Toupin's pioneering paper of 1956 [10]. His work was subsequently extended in a variety of ways by numerous authors, and most importantly for us by Tiersten to encompass deformable semiconductors [11]. The present effort builds on the latter work, adding in the consistent treatment of nonlinear electroelasticity to third order [12], [13], providing a more modern approach to the electrostatic boundary conditions, including the treatment of carrier recombination, emphasizing applications to the III-N materials, and generally seeking to make the approach more accessible to semiconductor device modelers.

To use a nonlinear theory for quantitative studies it is obviously necessary that the materials being modeled (which we assume to be of high quality) are well characterized, and that means having reliable values for the theory's various linear and nonlinear material coefficients. With regard to the linear coefficients, questions remain as to the "best" values, with theoretical ones often still being used that have not been thoroughly checked experimentally (and especially in the case of spontaneous polarization) [14]–[18]. For this paper we use the same linear coefficient values as in [6] with most of these being calculated ones obtained in [14]. Given that the linear coefficients have some uncertainty, it is no surprise that the nonlinear ones are even less well known, with very few experiments having been carried out to date [19], [20], and with most available values being calculated ones obtained using density functional theory [21]–[23]. Here we simply use the nonlinear coefficient values from [21], make no attempt to verify them or their derivation, and note only that it is possible to accurately measure them experimentally as has been done for certain strong piezoelectric materials like lithium niobate used in frequency control applications [24]. With regard to all of the assumed material coefficients, both linear and nonlinear, the reader should keep in mind their provisional nature, and especially when considering quantitative details of the illustrative simulations presented in Section IV.

The purpose of the present paper is to set out the nonlinear theory needed to treat large displacement/strain situations in piezoelectric semiconductors, and to apply it to various GaN device problems with the goals of illustrating the theory, assessing the sizes of the errors incurred by the linearization, and to the extent possible (again given that many of the nonlinear coefficients are not accurately known) gauging the importance of various nonlinear phenomena such as electrostriction. More broadly, it is hoped that this general framework might prove useful as a tool for analyzing other practical semiconductor devices in which "extreme" elastic states can serve a variety of electronic purposes such as mobility enhancement via band structure distortion, or for modeling semiconducting microelectromechanical (MEMS) devices that undergo large mechanical motions.

The paper is organized as follows. We begin in the next section with a detailed development of the nonlinear theory. The numerical approach is next described in Section III with emphasis on certain special issues that arise in the nonlinear case. The theory is then illustrated in Section IV with several technologically relevant examples, and the paper closes in Section V with some final remarks.

II. SEMICONDUCTORS WITH FINITE DEFORMATION

As noted in the Introduction, the first correct development of the equations of electroelasticity with finite deformation was given by Toupin in a paper that is a milestone in the history of modern classical field theory [10]. Because his work employed variational methods that have difficulties when dissipation is present, we here utilize a well known alternative that focuses directly on the basic conservation laws [11]–[13], [25]. For comprehensive coverage of the general principles and methods of classical field theory being used here, standard references should be consulted [8], [9]. Cartesian coordinates are used throughout, with vectors and tensors generally expressed in indicial notation with the Einstein summation convention assumed, and with indicial commas used to indicate partial differentiation. Coordinate-invariant notation is also used with vectors and tensors denoted in bold.

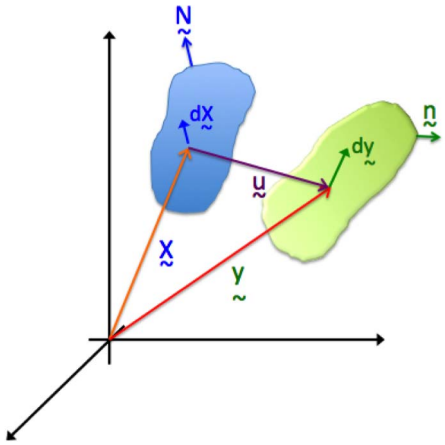

FIGURE 1. Schematic showing a generic object before (blue) and after (green) deformation with associated coordinates, displacement, and line elements.

In general, the mechanical deformation of a material can be described by the following mapping and its inverse:

$$y_i = y_i\,(X_1, X_2, X_3, t) \qquad X_L = X_L\,(y_1, y_2, y_3, t) \qquad (1)$$

where $i, L = 1, 2, 3$, and the vector field $\mathbf{y} = (y_1, y_2, y_3)$ gives the present position of the material in laboratory (or Eulerian) coordinates while the vector field $\mathbf{X} = (X_1, X_2, X_3)$ defines the reference position in a material (or Lagrangian) coordinate system as depicted in Fig. 1. As descriptions of the deformation, $(1)_1$ expresses how the present position $\mathbf{y}$ of a generic material point that was initially located at $\mathbf{X}$ evolves over time t, while $(1)_2$ gives the material coordinate X of a particular material point that is located at the generic laboratory coordinate $\mathbf{y}$ at time t. In these expressions we employ the standard convention in which the small letters (both the quantity and its index) denote Cartesian components in present coordinates, while the capital letters denote reference coordinate components. Under most circumstances it is reasonable to assume that away from boundaries the deformation is smooth, meaning that the functions defined in (1) are continuous and differentiable. This allows us to define the deformation gradient and its inverse by the respective two-point tensors:

$$F_{iL} \equiv y_{i,L} = \frac{\partial y_i}{\partial X_L} \quad \text{and} \quad X_{L,i} = \frac{\partial X_L}{\partial y_i} \qquad (2)$$

The determinant of the tensor $\mathbf{F}$ is the Jacobian J of the transformation in (1), *i.e.*,

$$J = det\,(\mathbf{F}) \tag{3}$$

and as such it measures the volume change that accompanies the deformation. Lastly, strain measures are defined based on (2) that (i) vanish when the material is unstrained (*i.e.*, when the deformation gradient is the identity matrix), and (ii) are rotationally invariant so that they do not change when the material is rotated in a fixed laboratory (or equivalently the material is held fixed and the laboratory is rotated). The standard quantities that meet these criteria are

$$S_{KL} = \frac{1}{2}\left(y_{i,K}y_{i,L} - \delta_{KL}\right) \qquad s_{ij} = \frac{1}{2}\left(\delta_{ij} - X_{K,i}X_{K,j}\right) \tag{4}$$

which are second-rank tensors called the Lagrangian (referred to reference coordinates) and Eulerian (referred to present coordinates) strains, respectively. Also note that to avoid any confusion with electric field, as in [6] we use $\mathbf{S}$ and $\mathbf{s}$ to denote strain rather than the conventional $\mathbf{E}$ and $\mathbf{e}$.

If V is an arbitrary but fixed volume with surface S and outward surface normal n_i, then the conservation of mass of the enclosed material can be written as:

$$\frac{d}{dt}\int_V \rho\ dV = 0 \tag{5a}$$

where ρ is the mass density. Similar equations for the conservation of charge in the electron and hole gases are

$$\frac{d}{dt}\int_V n\ dV = -\int_S n_i v_i^n\ dS - \int_V R\ dV \tag{5b}$$

$$\frac{d}{dt}\int_V p\ dV = -\int_S n_i p v_i^p\ dS - \int_V R\ dV \tag{5c}$$

where R is the net recombination rate (which could include photogeneration), n and p are the electron and hole densities, and v_i^n and v_i^p are the electron and hole velocities, respectively. That linear momentum is conserved in the lattice and in the electron and hole gases implies:

$$\frac{d}{dt}\int_V \rho v_i\ dV = \int_S t_i^M\ dS + \int_V \left(P_j E_{i,j} + q\left(N_D - N_A\right)E_i - qnE_i^n - qpE_i^p\right)\ dV \tag{5d}$$

$$0 = \int_S n_i p^n\ dS + \int_V qn\left(E_i - E_i^n\right)\ dV \tag{5e}$$

$$0 = \int_S n_i p^p\ dS - \int_V qp\left(E_i + E_i^p\right)\ dV \tag{5f}$$

where t_i^M is the mechanical stress traction vector, E_i is the electric field, $q(N_D - N_A)E_i$ and $P_j E_{i,j}$ are the forces (per unit volume) exerted by E_i on the ionized donor (N_D) and acceptor (N_A) densities and on the polarization P_i, respectively, $-qnE_i^n$ and $-qpE_i^p$ are the respective net forces (per unit volume) exerted by the electron and hole gases on the lattice as they flow through, and p^n and p^p are the electron and hole gas pressures, respectively. The conservation of energy for the collective lattice-electron-hole system may be written as:

$$\begin{aligned}
&\frac{\partial}{\partial t}\int_V \left[\rho\left(\varepsilon + \frac{1}{2}v_i v_i\right) + n\varepsilon^n + p\varepsilon^p\right] dV \\
&\quad + \int_S \rho n_j v_j\left(\varepsilon + \frac{1}{2}v_i v_i\right) dS + \int_S n n_i v_i^n \varepsilon^n dS + \int_S p n_i v_i^p \varepsilon^p dS \\
&= \int_S \left(t_i^M v_i - n_i p^n v_i^n - n_i p^p v_i^p - n_i q_i\right)\ dS \\
&\quad + \int_V \left(P_i E_{j,i} v_j + \rho E_i \frac{d\left(P_i/\rho\right)}{dt} + q\left(N_D - N_A\right)E_i v_i\right.\\
&\qquad \left. - qnE_i v_i^n + qpE_i v_i^p - H\right)\ dV
\end{aligned} \tag{5g}$$

where q_i is the heat flux vector and H is the power dissipated in recombination. Having the left side of (5*e*) and (5f) be zero and (5g) with no electron or hole kinetic energy terms means that we have neglected electron and hole inertia, an assumption that is almost always valid because of the very small size of the electron mass. (Situations where electron inertia can be important have been discussed in [26]). Finally, since this work employs the electrostatic approximation, Maxwell's equations reduce to

$$\int_S n_i D_i\ dS = \int_V q\left(N_D - N_A - n + p\right)\ dV \tag{5h}$$

$$-\int_S n_i \Psi\ dS = \int_V E_i\ dV \tag{5i}$$

where D_i is the electric displacement vector, Ψ is the electrostatic potential, and $D_i = \varepsilon_0 E_i + P_i$ where ε_0 is the permittivity of free space.

When the field variables are differentiable, *i.e.*, away from boundaries, the divergence theorem allows the integral forms in (5a-i) to be re-expressed as the following partial differential equations [8], [9], [12], [13]:

$$\rho_0 = J\rho \qquad \frac{dn}{dt} = \left(nv_i^n\right)_{,i} - R \qquad \frac{dp}{dt} = \left(pv_i^p\right)_{,i} - R \tag{6a}$$

$$\rho\frac{dv_j}{dt} = \tau_{ij,i}^M + P_i E_{j,i} - qnE_j^n - qpE_j^p + q\left(N_D - N_A\right)E_j \tag{6b}$$

$$0 = p_{,i}^n + qnE_i - qnE_i^n \qquad 0 = p_{,i}^p - qpE_i - qpE_i^p \tag{6c}$$

$$\begin{aligned}
&\rho\frac{d\varepsilon}{dt} + n\frac{d^n\varepsilon^n}{dt} + p\frac{d^p\varepsilon^p}{dt} - \tau_{ij}^M v_{j,i} + p^n v_{i,i}^n + p^p v_{i,i}^p \\
&\quad - \rho E_i\frac{d\left(P_i/\rho\right)}{dt} = qnE_i^n\left(v_i - v_i^n\right) + qpE_i^p\left(v_i - v_i^p\right)
\end{aligned} \tag{6d}$$

$$+ R\left(\frac{p^n}{n} + \varepsilon^n + \frac{p^p}{p} + \varepsilon^p\right) - H - q_{i,i}$$

$$D_{i,i} = q\left(N_D - N_A - n + p\right) \qquad E_i = -\Psi_{,i} \tag{6e}$$

where ρ_0 is the material mass density in reference coordinates, τ_{ij}^M is the mechanical stress tensor (which is related to the mechanical traction vector by $t_j^M = n_i\tau_{ij}^M$), $J_i^n \equiv nv_i^n$ and $J_i^p \equiv pv_i^p$ are the electron and hole number current densities, $d/dt \equiv \partial/\partial t + v_i\partial/\partial y_i$ is the material derivative following the lattice, $v_i \equiv \partial y_i/\partial t$ is the lattice velocity, and $d^n/dt \equiv \partial/\partial t + v_i^n\partial/\partial y_i$ and $d^p/dt \equiv \partial/\partial t + v_i^p\partial/\partial y_i$ are the

material derivatives following the electron and hole gases, respectively.

For formulating boundary conditions it is useful to re-write (6b) in terms of the electrostatic Maxwell stress tensor τ_{ij}^E as

$$\rho\frac{dv_j}{dt} = \tau_{ij,i}^M + \tau_{ij,i}^E - p_{,j}^n - p_{,j}^p$$
$$\text{where} \quad \tau_{ij}^E = \varepsilon_0 E_i E_j + P_i E_j - \frac{\varepsilon_0}{2} E_k E_k \delta_{ij} \tag{7}$$

The last two term on the right hand side of $(7)_1$ represent the pressures exerted by the electron and hole gases on the lattice. For a crude estimate, according to the Maxwell-Boltzmann formula (see $(22b)_1$ below) an electron density of $10^{20}/\text{cm}^3$ will produce a pressure of about 0.4MPa, and since we are interested in problems where the electromechanical stresses are 1GPa and more, one is justified in following the conventional (and always implicit) assumption of neglecting the electron and hole pressure contributions to the lattice deformation.

In addition to the differential equations in (6a-e) and (7) the field theory must also specify boundary conditions. In order to ensure their consistency with the differential equations, these conditions are derived from the same integral forms in (5a-i) by applying them to a "Gaussian pillbox" that is bisected by a surface of discontinuity and taking appropriate limits [8], [9]. In this way, the following boundary conditions are readily derived:

$$[\psi] = 0 \qquad n_i [D_i] = \sigma \qquad n_i \left[\tau_{ij}^M + \tau_{ij}^E\right] = 0$$
$$n_i \left[J_i^n\right] = 0 \qquad n_i \left[J_i^p\right] = 0 \tag{8}$$

where the brackets denote the jump in value across the interface when going in the direction of the normal vector **n** and the electron and hole pressure terms in (7) have been neglected in deriving $(8)_3$. In the special case of external surfaces, charge will accumulate over time and result in these surfaces being neutralized; this assumption is also often applied at internal surfaces, *e.g.*, at III-N surfaces on which silicon nitride is deposited by CVD methods, but in this case the compensation is often not perfect [27]. To represent the neutralization, we note that the total surface charge is

$$\sigma_{tot} = n_i [\varepsilon_0 E_i] = \sigma - n_i P_i \tag{9a}$$

and since the neutrality requirement is $\sigma_{tot} = 0$, (9a) implies

$$n_i [D_i] = n_i P_i \tag{9b}$$

The equations in (6a-e), (7), (8) and (9b) are general expressions of the governing physical principles, namely, the conservation laws, electrostatics, and thermodynamics. But they do not yet contain the specific material response functions that express characteristics such as the elastic stiffness, the piezoelectric coupling, or the electron mobility. These functions, also called constitutive equations, are not arbitrary but rather are constrained in form by the thermodynamics and by various symmetry and invariance conditions whose proper treatment in electroelasticity is due to Toupin [10]. Because the electroelastic and electron/hole pressure interactions are non-dissipative in nature, many of these material response functions are derivable from an electric Gibbs free energy function Ψ [28] and from electron and hole stored energy functions, ε^n and ε^p [6], [11]. To this end, from (6d) we write the second law of thermodynamics for our system as [9], [10]:

$$\rho\frac{d\Psi}{dt} + n\frac{d^n\varepsilon^n}{dt} + p\frac{d^p\varepsilon^p}{dt} + P_i\frac{dE_i}{dt} - \tau_{ij}^M v_{j,i} + p^n v_{i,i}^n + p^p v_{i,i}^p = -\rho\eta\frac{dT}{dt} \tag{10a}$$

where $\rho\Psi = \rho\varepsilon - \rho\eta T - P_i E_i$, ε is the stored energy in the lattice per unit mass, and η is the lattice entropy per unit mass. That the total stored energy can be split cleanly into "lattice" and "electron gas" contributions is a basic assertion of the theory developed in this paper. Combining (6d) and (10a) gives the dissipation equation that governs heat conduction

$$\rho T\frac{d\eta}{dt} + q_{i,i} = qnE_i^n\left(v_i - v_i^n\right) + qpE_i^p\left(v_i - v_i^p\right) + R\left(\frac{p^n}{n} + \varepsilon^n + \frac{p^p}{p} + \varepsilon^p\right) - H \tag{10b}$$

where the first two terms on the right hand side are the Joule heating associated with electron and hole scattering that convert mechanical energy to thermal energy when there is relative motion between the carrier gases and the lattice, and the last two terms represent dissipation and entropy production associated with recombination. From (10b), the Clausius-Duhem inequality takes the form

$$\rho\frac{d\eta}{dt} + \left(\frac{q_i}{T}\right)_{,i} = -\frac{1}{T}\left[\frac{q_i T_{,i}}{T} - qnE_i^n\left(v_i - v_i^n\right) - qpE_i^p\left(v_i - v_i^p\right) - R\left(\frac{p^n}{n} + \varepsilon^n + \frac{p^p}{p} + \varepsilon^p\right) + H\right] \geq 0 \tag{10c}$$

where the right hand side is called the rate of entropy production and the inequality represents the proscription on decreasing entropy within the field theory [8], [9].

Using the identities $v_{j,i} = X_{L,i}d(y_{j,L})/dt$ and $v_{i,i}^n = -(1/n)d^n n/dt$ we can re-write (10a) as

$$\rho\frac{d\Psi}{dt} + P_i\frac{dE_i}{dt} - \tau_{ij}^M X_{L,i}\frac{dy_{j,L}}{dt} + n\frac{d^n\varepsilon^n}{dt} + p\frac{d^p\varepsilon^p}{dt} - \frac{p^n}{n}\frac{d^n n}{dt} - \frac{p^p}{p}\frac{d^p p}{dt} + \rho\eta\frac{dT}{dt} = 0 \tag{11a}$$

And from the form of (11a) and the assumed clean separation of lattice and electron gas energies we conclude that

$$\Psi = \Psi\left(y_{i,L}, E_i, T\right) \qquad \varepsilon^n = \varepsilon^n(n,T) \qquad \varepsilon^p = \varepsilon^p(p,T) \tag{11b}$$

Inserting (11b) into (11a) and applying the chain rule leads to[1]

$$0 = \left[\tau_{ij}^{M} X_{L,i} - \rho\frac{\partial\Psi}{\partial y_{j,L}}\right]\frac{dy_{j,L}}{dt} - \left[P_i + \rho\frac{\partial\Psi}{\partial E_i}\right]\frac{dE_i}{dt} + \left[\frac{p^n}{n} - n\frac{\partial\varepsilon^n}{\partial n}\right]\frac{d^n n}{dt} + \left[\frac{p^p}{p} - p\frac{\partial\varepsilon^p}{\partial n}\right]\frac{d^p p}{dt} - \rho\left[\eta + \frac{\partial\Psi}{\partial T}\right]\frac{dT}{dt} \tag{11c}$$

For the equality in (11c) never to be violated it must hold for arbitrary values of the time derivatives, and so each quantity in brackets must separately vanish, *i.e.*,

$$\tau_{ij}^{M} = \rho y_{i,L}\frac{\partial\Psi}{\partial y_{j,L}} \qquad P_i = -\rho\frac{\partial\Psi}{\partial E_i} \qquad p^n = n^2\frac{\partial\varepsilon^n}{\partial n}$$
$$p^p = p^2\frac{\partial\varepsilon^p}{\partial p} \qquad \eta = -\frac{\partial\Psi}{\partial T} \tag{12}$$

The expressions in (12) are the constitutive equations that become explicit when functional forms for the energies in (11b) are specified.

Now a crucial observation of finite deformation theory is that $\Psi = \Psi(y_{i,L}, E_i, t)$ cannot be an arbitrary function of its arguments because this would lead to violations of rotational invariance, *i.e.*, a material's properties could change simply as a result of it being rotated [10]. To guarantee against such violations, a theorem of Cauchy [8], [9] requires that the dependences on $y_{i,L}$ and E_i be through rotationally invariant products of these terms. One such product is the Lagrangian strain tensor S_{LM} as defined in $(4)_1$ and a similar invariant involving the electric field is the product

$$W_L \equiv y_{i,L}E_i \tag{13}$$

No similar restrictions arise for ε^n and ε^p since they have only scalar dependences (which are of course unchanged by rotation). Based on the foregoing, we therefore restrict the form of the electric Gibbs free energy of $(11b)_1$ to be

$$\Psi = \Psi\left(S_{LM}, W_L, t\right) \tag{14a}$$

A further application of the chain rule with $(4)_1$ then leads to the following replacements for the first two equations in (12):

$$\tau_{ij}^{M} = \frac{1}{J}y_{i,L}y_{j,M}\tau_{LM} - P_i E_j \qquad P_i = \frac{1}{J}y_{i,L}P_L \tag{14b}$$

$$\text{where} \qquad \tau_{LM} = \rho_0\frac{\partial\Psi}{\partial S_{LM}} \qquad P_L = -\rho_0\frac{\partial\Psi}{\partial W_L} \tag{14c}$$

are reference coordinate expressions for the total (or second Piola-Kirchoff) stress tensor and the polarization vector.

1. For reasons of simplicity, entropy contributions associated with temperature derivatives of ε^n and ε^p are neglected from (9c) because they would lead to defining a separate temperature and entropy for the electron gas. Also, the temperature dependences in $(11b)_2$ and $(11b)_3$ produce thermoelectric effects associated with the electron gas, and our treatment requires that entropy carried by such current be negligible.

Inserting $(14b)_1$ into (7) allows the governing momentum balance equation to be put in the symmetrized form

$$\rho\frac{d^2 y_j}{dt^2} = \left[\frac{1}{J}y_{i,L}y_{j,M}\tau_{LM} + \tau_{ij}^{ES}\right]_{,i}$$
$$\text{where} \quad \tau_{ij}^{ES} = \varepsilon_0 E_i E_j - \frac{\varepsilon_0}{2}E_k E_k \delta_{ij} \tag{15a}$$

is the free-space Maxwell electrostatic stress tensor, and as justified earlier the forces exerted by the electron and hole gases on the lattice in (7) have been neglected. Similarly, using $(6e)_2$ and $(14b)_2$, $(6e)_1$ can be re-written as

$$\left[-\varepsilon_0\psi_{,i} + \frac{1}{J}y_{i,L}P_L\right]_{,i} = q\left(N_D - N_A - n + p\right) \tag{15b}$$

One other standard convenience of diffusion-drift theory comes from defining chemical potentials φ^n and φ^p by [5], [9]

$$\varphi^n = \frac{\partial\left(n\varepsilon^n\right)}{\partial n} \qquad \varphi^p = \frac{\partial\left(p\varepsilon^p\right)}{\partial p} \tag{16a}$$

with which (6c) can be re-written as

$$0 = \varphi_{,i}^n + E_i - E_i^n \qquad 0 = \varphi_{,i}^p - E_i - E_i^p \tag{16b}$$

Finally, in addition to the non-dissipative equations generated from (14c) with (14a) and (16a) with $(11b)_2$ and $(11b)_3$, there are also a few dissipative constitutive equations that arise from the demand that (10c) be satisfied under all circumstances. To lowest order these equations take the forms:

$$E_i^n = \frac{v_i - v_i^n}{\mu_n} \qquad E_i^p = \frac{v_i - v_i^p}{\mu_p} \qquad q_i = q_i\left(T_{,j}\right) \tag{17a}$$
$$R = R\left(n, p\right) \qquad H = H\left(n, p\right) \tag{17b}$$

where μ_n and μ_p being the electron and hole mobilities. Since the *relative* motion of the electron and hole gases are rotationally invariant, $(17a)_1$ and $(17a)_2$ need not involve material coordinates; of course, one could make the mobilities tensors if one wished to include a dependence on crystal orientation. As in (13), to ensure the rotational invariance of the heat conduction in $(17a)_3$ we define a new variable $G_K = y_{i,K}T_{,j}$ and $(17a)_3$ in reference coordinates is then written as:

$$q_K = q_K\left(G_L\right) = -\kappa_{KL}G_L \tag{17c}$$

where the second equality is the linear (Fourier) approximation. The requirement that (10c) always be satisfied implies that μ_n, μ_p, and κ_{KL} are all non-negative. In addition, we should have:

$$H \geq \left(\frac{p^n}{n} + \varepsilon^n + \frac{p^p}{p} + \varepsilon^p\right) \qquad R = \left(\varphi^n + \varphi^p\right)R \tag{17d}$$

where the equality on the right follows from (16a).

The development so far has laid out the general formulation of the nonlinear continuum theory of piezoelectric semiconductors. In addition to the usual electrical nonlinearities of a semiconductor that

were already included in [6], *i.e.*, those contained in (6a), $(11b)_2$, $(11b)_3$, (16a,b), $(17a)_1$, $(17a)_2$, and $(17b)_1$, the present theory also includes nonlinearities that arise from the electromechanics. These occur in five main areas as highlighted below.

(i) Maxwell stress: Being quadratic in the electric field, the free-space Maxwell stress exerted by the electrostatic field on the lattice does not enter the linear theory. But consistency demands that it be included in the nonlinear theory as emphasized in (15a).

(*ii*) *Kinematic nonlinearities:* The second difference from linear theory enters through the so-called kinematic nonlinearities associated with nonlinear terms in the Lagrangian strain in $(4)_1$ and in the reference forms for the electric field in (13) and the temperature gradient in (17c). To display these corrections explicitly, define a displacement vector as (see Fig. 1)

$$u_i \equiv y_i - X_L \delta_{Li} \tag{18a}$$

with which $(5)_1$, (11), and (15c) become

$$\begin{aligned} S_{KL} &= \frac{1}{2}\left(u_{i,L}\delta_{Ki} + u_{i,K}\delta_{Li} + u_{i,K}u_{i,L}\right) \\ W_K &= \left(\delta_{Ki} + u_{i,K}\right)E_i \qquad G_K = \left(\delta_{Ki} + u_{i,K}\right)T_{,i} \end{aligned} \tag{18b}$$

the first two terms in $(18b)_1$ and the first terms in $(18b)_2$ and $(18b)_3$ represent the ordinary linearized strain, electric field, and temperature gradient, respectively, as used for example in [6]. And the last terms in $(18b)_1$, $(18b)_2$, and $(18b)_3$ are the additional kinematic nonlinearities that enter the nonlinear theory and are included in the calculations of this paper (Section IV).

(*iii*) *Constitutive nonlinearities:* The third set of differences between the linear and nonlinear theories are referred to as constitutive nonlinearities and they arise when higher-order terms are included in the various constitutive equations, and especially the electromechanical contributions that enter via the function Ψ in (14a). For this paper we include elastic and electric terms consistently to third order using a "power series" form [12], [13]:

$$\begin{aligned} &\rho\Psi\left(S_{KL}, W_K, n, T\right) \\ &= \rho c_p T\left[1 - \ln\left(T/T_0\right)\right] + \tau^0_{KL}S_{KL} - P^0_K W_K + \lambda_K W_K\left(T - T_0\right) \\ &\quad + C_{KLMN}S_{KL}\left[\frac{1}{2}S_{MN} - \alpha_{MN}\left(T - T_0\right)\right] - \frac{1}{2}\chi_{KL}W_K W_L \\ &\quad - e_{KLM}W_K S_{LM} - \frac{1}{2}b_{KLMN}W_K W_L S_{MN} - \frac{1}{6}\chi_{KLM}W_K W_L W_M \\ &\quad - \frac{1}{2}k_{KLMND}W_K S_{ND}S_{LM} + \frac{1}{6}C_{KLMNDE}S_{KL}S_{MN}S_{DE} \end{aligned} \tag{19}$$

where the last four terms on the right side are those beyond what were included in [6] and represent the constitutive nonlinearities. (Beyond these terms, in order to describe ferroelectric hysteresis, *e.g.*, as seen in [29], a fourth-order susceptibility term would need to be included in (19). Also note that with both pyroelectricity and piezoelectricity considered, there can be both proper and improper coefficients; our formulation considers only the latter [18], [30].) The material constants C_{KLMN}, C_{KLMNAB}, χ_{KL}, χ_{KLM}, γ, e_{KLM}, k_{KLMAB}, b_{KLMN}, α_{MN}, and λ_K are the second- and third-order elastic, second- and third-order electric susceptibility, specific heat, piezoelectric, first odd electroelastic, electrostrictive, thermal expansion, and pyroelectric coefficients, respectively, the quantities τ^0_{KL} and P^0_K are the intrinsic (or built-in) stress and polarization, respectively, and T_0 is a reference temperature. The components of the various material tensors in (19) are not all independent, but instead are strongly constrained by the need to match the symmetries of the crystal. In particular, because the wurtzite III-N materials of interest in this paper belong to the hexagonal point group *6mm*, the associated constraints on the various tensor components imply that of the 9 coefficients α_{MN} just two are independent, and similarly the number of independent coefficients among the χ_{KL} are two, among the e_{KLM} and χ_{KLM} there are three each, among the C_{KLMN} there are five, among the b_{KLMN} there are six, among the k_{KLMAB} there are eight, and among the C_{KLMNAB} there are ten (see the Appendix for more detail) [30]. As noted in the Introduction, many of the material coefficient values are not well known, and this may include the linear ones that we here assume to take the literature values used in [6]. For the nonlinear coefficients we use values taken mostly from the density functional theory calculations of [21] and summarized in Table 1. That these coefficient values are not definitively established and could well have significant errors should be kept in mind, and particularly when considering the illustrative device simulations presented in Section IV.

TABLE 1. Non-linear material coefficients [21]

	GaN	AlN		GaN	AlN
χ_{113}(pm/V)	-4	0.24	k_{333} (C/m^2)	-23.4	-25.6
χ_{333}(pm/V)	6	-4	k_{115} (C/m^2)	6.48	8.69
C_{111} (GPa)	-1225	-1525	k_{125} (C/m^2)	5.09	5.19
C_{112} (GPa)	-834	-374	k_{135} (C/m^2)	7.02	3.2
C_{113} (GPa)	-283	-66	k_{344} (C/m^2)	1.41	2.88
C_{123} (GPa)	-631	-688	b_{11}/ε_0	23.3	11.9
C_{133} (GPa)	-967	-1117	b_{12}/ε_0	9.8	8.9
C_{222} (GPa)	-974	-271	b_{13}/ε_0	11.2	7.3
C_{333} (GPa)	-1126	-56	b_{31}/ε_0	27.6	37.4
k_{311} (C/m^2)	6.26	3.77	b_{33}/ε_0	-84.4	-73.6
k_{312} (C/m^2)	2.37	4.12	b_{44}/ε_0	9.9	3.6
k_{313} (C/m^2)	-1.47	-8.64			

By inserting (19) into (14c) we derive the following expressions for the stress tensor and the polarization vector:

$$\begin{aligned} \tau_{KL} &= \tau^0_{KL} + C_{KLMN}\left[S_{MN} - \alpha_{MN}\left(T - T_0\right)\right] - e_{MKL}W_M \\ &\quad - \frac{1}{2}b_{KLMN}W_M W_N - k_{MKLND}W_M S_{ND} \\ &\quad + \frac{1}{2}C_{KLMNDE}S_{MN}S_{DE} \end{aligned} \tag{20a}$$

$$P_K = P_K^0 - \lambda_K (T - T_0) + \chi_{KL} W_L + e_{KLM} S_{LM} + b_{KLMN} W_L S_{MN} + \chi_{KLM} W_L W_M + \frac{1}{2} k_{KLMND} S_{LM} S_{ND} \tag{20b}$$

Also, when (19) with $(17a)_1$ and $(17a)_2$ is inserted into $(10b)$ the following form for the heat equation results:

$$\rho c_p \frac{dT}{dt} + q_{i,i} = \frac{qn}{\mu_n}\left(v_i - v_i^n\right)^2 + \frac{qp}{\mu_p}\left(v_i - v_i^p\right)^2 \tag{21a}$$

$$\text{where} \quad q_{i,i} = \left[\frac{1}{J} y_{i,L} q_L\right]_{,i} = -\left[\frac{1}{J} y_{i,L} y_{j,M} \kappa_{LM} T_{,j}\right]_{,i} \tag{21b}$$

and the right side of (21a) is the Joule heating arising from the motion of the electron and hole gases relative to the lattice.

Although electrical nonlinearities are not emphasized in this paper, we nevertheless note that the simplest expressions for the electron and hole energies ε^n and ε^p in $(11b)_2$ and $(11b)_3$ are those associated with the Maxwell-Boltzmann distribution:

$$\frac{\varepsilon^n(n,T)}{k_B T} = \ln\left(\frac{n}{n_i}\right) - 1 \qquad \frac{\varepsilon^p(p,T)}{k_B T} = \ln\left(\frac{p}{n_i}\right) - 1 \tag{22a}$$

The expressions for the electron and hole pressures and the electron and hole chemical potentials that result from inserting (22a) into $(12)_3$ and $(12)_4$ with (16a) are then:

$$p^n = k_B T n \qquad \varphi^n = E_C - E_i + k_B T \ln\left(\frac{n}{n_i}\right) \tag{22b}$$

$$p^p = k_B T p \qquad \varphi^p = E_i - E_V + k_B T \ln\left(\frac{p}{n_i}\right) \tag{22c}$$

where E_C, E_V, E_i, and n_i have their usual meanings. That the electron and hole pressures are proportional to the electron and hole densities, respectively, shows that the stored energy functions in (22a) are those appropriate for linear theory. For most real device problems, these expressions are not sufficient and constitutive nonlinearities must be added to account for high-density effects like those due to Fermi-Dirac statistics and energy band non-parabolicity. Because such corrections are well known [31], they are not discussed further here, but are included in the simulations of Section IV. Lastly note that in the Maxwell-Boltzmann approximation, (17b) combined with (22a-c) yields $H \geq R[E_G + k_B T\, ln(np/n_i^2)]$ which says that the dissipated energy (per electron-hole pair) associated with recombination is greater that or equal to the average band-to-band energy.

(*iv*) *Carrier recombination:* Being an ordinary nonlinearity of semiconductors, carrier recombination merits further attention only because it involves a special kinematic nonlinearity. To see this, consider a typical expression for the recombination rate of the form:

$$R = \frac{np - n_{eq} p_{eq}}{\tau} \tag{23a}$$

where τ is the carrier lifetime. As is well known, equilibrium statistical mechanics provides relationships $n_{eq} = f_n(\psi_{eq}, T)$ and $p_{eq} = f_p(\psi_{eq}, T)$ and if no mechanical deformation is present or such deformations are treated with linear theory, then no more is needed and all is as in the conventional case. But for nonlinear theory one must keep track of the deformed states under *both* equilibrium and non-equilibrium conditions, *i.e.*, without or with electrical bias, current, and recombination (and in both cases with all external forces applied). If the solution for the deformed state in equilibrium is given by $\boldsymbol{y}_{eq} = \boldsymbol{y}_{eq}(\boldsymbol{X})$, then in present coordinates (23a) will be replaced by

$$R(\boldsymbol{y}, t) = \frac{n(\boldsymbol{y}, t)\, p(\boldsymbol{y}, t) - n_{eq}\left(\boldsymbol{y}_{eq}(\boldsymbol{X}(\boldsymbol{y}, t))\right) p_{eq}\left(\boldsymbol{y}_{eq}(\boldsymbol{X}(\boldsymbol{y}, t))\right)}{\tau} \tag{23b}$$

where $n_{eq}(\boldsymbol{y}_{eq})$ and $p_{eq}(\boldsymbol{y}_{eq})$ are the solutions for the equilibrium densities. This gets further complicated if there is an applied mechanical force that varies with time since then the "equilibrium" solutions for the deformation and the carrier densities will be quasistatic and will also vary with time.

(*v*) *Boundary conditions:* The boundary conditions in (8) and (9b) are much like those of the linear theory (*e.g.,* [6]), though of course with extra contributions from constitutive nonlinearities. As such, they deserve further discussion only because a special type of kinematic nonlinearity can arise, specifically when the electrostatic boundary conditions $(8)_1$ and $(8)_2$ are applied at external boundaries where the semiconductor or other materials about the air or vacuum. In the linear theory, the small size of the deformation means that one can ignore the movement of these external boundaries, but this is not true in the case of finite deformations and then the treatment is no longer as straightforward as was emphasized in [12] and [13]. One way of describing the difficulty is that there is no deformation in the air/vacuum and therefore there is no mapping like (1) with which to transform the electrostatic variables in the air/vacuum into reference coordinates where the surface position is known (and where only electrostatic variables are of concern because they are the only field variables that exist in the air/vacuum). Tiersten [12], [13] proposed handling this conundrum by estimating these electrostatic variables using Taylor expansions. But a much better way is simply to apply the known electrostatic boundary conditions at the unknown present position of the interface, which then becomes part of the solution as discussed below. And it is precisely for this reason that the equations to be solved as given in (15a), (15b), and (21) have been formulated in *present* coordinates rather than in *reference* coordinates.

To summarize, when $(6a)_1$, $(6e)_2$, $(11b)_2$, $(11b)_3$, (16a), $(17a)_1$, $(17a)_2$, (18b), (20a), (20b), (21b) and (23b) are inserted into $(6a)_2$, $(6a)_3$, (15a), (15b), (16b), and (21a) we obtain (in three dimensions) seven scalar PDEs in

present coordinates in the seven unknowns u_i, ψ, n, p, and T. This full set of equations obviously applies only to semiconductors; in solid insulators no electron transport is allowed, in metals only heat conduction occurs, and in the surrounding air/vacuum only electrostatics applies. These differential equations, together with the boundary conditions in (8) and (9b), can be used to formulate boundary value problems appropriate to devices of interest, and their solution then allows the device properties to be understood and engineered (as illustrated in Section IV). Because of the complexity of the geometries, material properties, and governing equations (especially in the nonlinear case), these solutions almost always require numerical methods, and this aspect is discussed in the next section.

III. NUMERICAL APPROACH

To obtain numerical solutions to the boundary value problems formulated within the nonlinear theory of Section II, we employed the powerful COMSOL package [32] as we did in our earlier work [6]. This general-purpose program uses the finite element method on unstructured grids. The main aspect in need of discussion is various assumptions, simplifications, and "tricks" we invoke to keep the computational burden manageable on a desktop computer.

One basic assumption taken for computational efficiency is that we confine our study to "wide" devices for which a 2D plane-strain treatment would seem appropriate. However, the matter is not entirely straightforward because the strain fields in III-N devices are usually three-dimensional as a result of biaxial stresses that are imposed by heteroepitaxy. For linear problems this is not a problem since one can simply subtract off the known epitaxial strain field analytically [6], but such a procedure will not in general be valid in the nonlinear case. Nevertheless, for reasons of simplicity, we assume that the deformation in the width direction is well approximated by that produced solely by the epitaxy. Denoting the epitaxial deformation in the plane of layer k by $\xi_i^{(k)}$ $(i = 1, 2)$, the associated deformation gradient will be:

$$\xi_{i,L}^{(k)} \equiv \begin{cases} a_k \delta_{iL}/a_{sub}, & i = 1, 2 \\ 0, & i = 3 \end{cases} \tag{24}$$

where a_k and a_{sub} are the in-plane lattice constants of the k^{th} layer and the unstrained substrate, respectively. (The in-plane strain will also induce a "Poisson ratio" deformation in the 3-direction but this will be included automatically in the plane-strain solution). The strain expression in $(4)_1$, the electric field expression in (11), and the temperature gradient expression in (17) will then take the forms:

$$S_{KL}^{(k)} = \frac{1}{2}\left[\left(\hat{y}_{i,K} + \xi_{i,K}^{(k)}\right)\left(\hat{y}_{i,L} + \xi_{i,L}^{(k)}\right) - \delta_{KL}\right] \tag{25a}$$

$$W_L = \left(\hat{y}_{i,L} + \xi_{i,L}^{(k)}\right) E_i \qquad G_L = \left(\hat{y}_{i,L} + \xi_{i,L}^{(k)}\right) T_{,i} \tag{25b}$$

where $\hat{y}_i = y_i - \xi_i^{(k)}$. The expressions in (25) are completely general, and the simplifying assumption enters only in the taking of $\hat{y}_i$ to be a pure 2-D plane-deformation with $\hat{y}_2 \cong \hat{y}_{1,2} \cong \hat{y}_{3,2} \cong 0$.

A second simplification we employ arises from the fact that the semiconductor equations generally require much finer grids than do the mechanical and thermal variables, e.g., to resolve very thin boundary layers in the carrier density such as the accumulation layer at an AlGaN/GaN interface. This issue is exacerbated by the fact that we do not use the exponential-fitting (Scharfetter-Gummel) scheme commonly employed in device modeling in order to stabilize the discretization of the semiconductor nonlinearity, and thereby relax grid requirements [31]. For these reasons, for most problems we improve the computational efficiency by following [6] in solving for the mechanical/thermal variables over the full structure while restricting the electrical solutions to much smaller "active" regions. This strategy is depicted in Fig. 2 for the simulation of a conventional AlGaN/GaN HEMT. Obviously one can check on the validity of such an approach simply by varying the size of the "active" region and looking for discrepancies in the solutions so obtained.

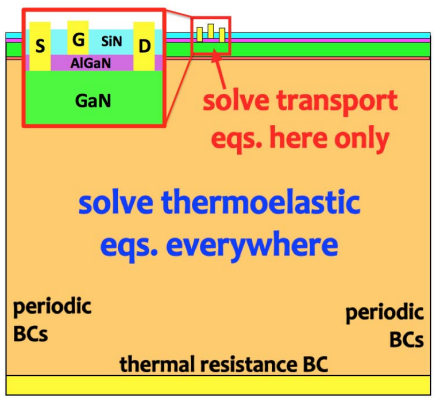

FIGURE 2. Schematic of an AlGaN/GaN HEMT and a depiction of the simulation strategy.

Another numerical issue deserving comment is the existence of singularities in the solutions at corners. These spurious singularities arise from the continuum treatment of an ideal corner, and, being unphysical, are of no interest unless they corrupt the overall solution or one is interested in estimating the maximum field value. As discussed previously in [6], these singularities can be handled by imposing a cut-off distance (taken to be 1Å in [6]) and resolving the behavior in the vicinity of the corner only outside of this cut-off. In the present paper we used this approach as well, but alternatively introduce tightly filleted corners when appropriate in order to eliminate the associated singularity entirely.

As noted in the previous section, in nonlinear electroelastic theory one needs to be careful in applying the electrostatic conditions at external boundaries. The neatest and most generally useful way of handling things is to solve the equations in present coordinates with the unknown positions of the external boundaries then becoming part of the solution. To carry this out requires using a so-called Lagrangian mesh

that follows the material. The COMSOL code [32] is especially convenient in this regard because it includes a built-in implementation of the arbitrary Lagrangian-Eulerian (ALE) technique [33] for producing useful grids for a wide variety of applications in solid and fluid mechanics. In our usage, we simply employ the full Lagrangian limit. Also, to avoid the complications of contact problems (including limitations of COMSOL), we do not consider the interesting situations in which initially separate surfaces come into contact as a result of large deformations.

With the foregoing "tricks" implemented, the simulations generally run with reasonable efficiency and with good convergence. For the latter, as is typical in device simulation (and characteristic of a Newton iteration scheme), it is important that one have a "good" initial guess. In our work this is generally provided by continuation from purely electrical solutions with no deformation or temperature. The main threat to stability is the familiar one of semiconductor device modeling associated with the strong electrical nonlinearity of the semiconductor equations, and for this the key (as is well known) is having a fine enough grid in regions in which the potential varies substantially. As noted earlier, this issue is exacerbated in our simulations because we have not implemented the Scharfetter-Gummel discretization. Nevertheless, as long as the device size is not too great, 2D simulations are readily accomplished on a single-processor desktop computer with run times that are not overly long. Furthermore, if the approach were to be carried into an engineering environment, there are a number of obvious aspects that could be optimized, e.g., implementing Scharfetter-Gummel or using multi-core processing, to further improve run times. This would also be needed if one wished to analyze devices in 3D.

IV. APPLICATIONS

This section discusses three areas of application of the nonlinear theory with two primary goals in mind. The first is to examine the size of the nonlinear corrections and thereby to assess the errors made by linear simulations in various circumstances including those of conventional HEMTs. And the second purpose is to illustrate the value of the nonlinear formulation, especially for certain types of problems such as those relating to MEMS devices in which large rotations occur. For all of these illustrative simulations, again a main caveat is that the values of the material coefficients, and especially the nonlinear ones obtained from [21], could well have significant errors.

(i) Conventional GaN HEMTs: As a first set of calculations, in this sub-section we compare linear and nonlinear simulations of conventional GaN HEMTs for the purpose of assessing the importance of the nonlinear corrections in "ordinary" GaN device situations. To begin we treat a microwave AlGaN/GaN device structure as depicted in Fig. 2 with a gate length of 0.3μm, an Al fraction of 30%, an AlGaN thickness of 20nm, a SiN passivation layer that is 50nm thick, a lateral spacing between gates of 125μm, and $\phi_m - \Delta E_C \cong 0.81$ [34]. (It should be noted that in [6] $\phi_m - \Delta E_C$ was assumed to be 2.6eV simply in order to get a threshold voltage of around 4V, that corresponded well with measurement). The simulated drain and transfer characteristics are shown in Figs. 3a and 3b, respectively, with results from both linear and nonlinear theories included. From their comparison it is clear that the nonlinear corrections are significant, with the main impact being a threshold voltage shift of about 0.5V. To understand the origin of this nonlinear correction, a series of further simulations was carried out in which each nonlinear term was turned on one at a time, and the threshold voltage contributions from each were thereby ascertained, with the results depicted in Fig. 4. Evidently the shift arises mainly from constitutive nonlinearities, and in particular from the third-order electroelastic effect and from electrostriction. This also implies that errors in these particular coefficient values would be most impactful on the results. To see where in the device the aggregate polarization and stress corrections are most important, in Figs. 5a and 5b we plot the relative sizes of the respective nonlinear terms as compared to the totals. Not surprisingly, these simulations show that the nonlinear contributions are largest in the strained AlGaN barrier, with the stress nonlinearities showing more "leakage" into the GaN channel. The threshold voltage shift of Fig. 3(bottom) is in part due to the AlGaN effects and their influence on the polarization charge at the interface, but the direct effect in the GaN on the channel charge also contributes.

A second conventional device examined in simulation was of a millimeter-wave AlN/GaN HEMT with a vertically scaled barrier and with higher strains due to the greater lattice mismatch between the binaries [35]. The simulated transfer

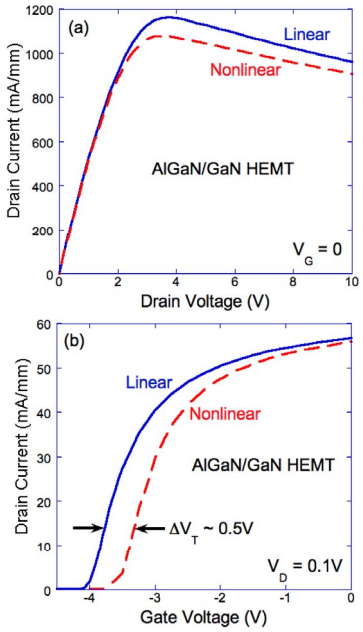

FIGURE 3. Simulated (a) drain and (b) transfer characteristics of a GaN HEMT comparing the nonlinear result with that computed with linear theory.

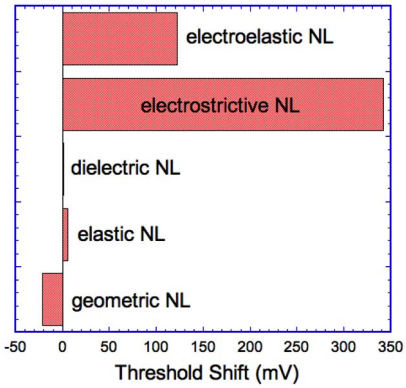

FIGURE 4. **Contributions of various nonlinear terms to the threshold voltage shift seen in Fig. 3b. Constitutive nonlinearities are seen to dominate in this situation.**

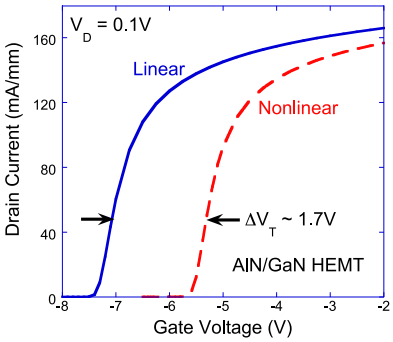

FIGURE 6. **Simulated transfer characteristics of a AlN/GaN HEMT comparing the nonlinear result with that computed with linear theory.**

characteristics for this device (with the device dimensions remaining the same except for the AlN thickness being 7.5nm and with $\phi_m - \Delta E_C \cong 0.24$ [34]) are shown in Fig. 6. Not unexpectedly, the increase in strain is found to boost the size of the nonlinear correction with the threshold voltage now shifted by about 1.7V. The origins of this shift are much the same as in the AlGaN/GaN HEMT described in Figs. 4 and 5.

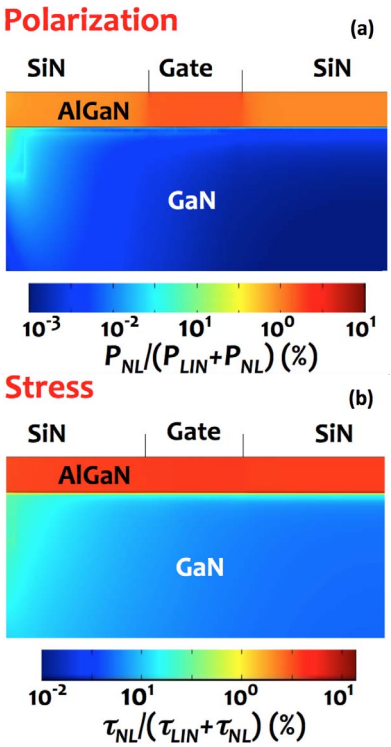

FIGURE 5. **Logarithmic field plots of the relative contributions of the nonlinear terms to (a) polarization and (b) stress in an AlGaN/GaN HEMT with $V_D = 0.1$ V. The variations on the left side of these plots arise from the proximity of the source.**

The contributions of nonlinearity to the threshold voltages seen in the HEMT simulations in Figs. 3b and 6 are quite large, again with the caveat regarding the accuracy of the material coefficient values. Given their size, it seems safe to say that *nonlinearity cannot be neglected when modeling conventional* HEMTs. Furthermore, it would seem that prior simulation work with linear theory, *e.g.,* [5], [6], and [33], was effective solely because the effect of the nonlinearity in the HEMT problem is almost entirely restricted to the threshold voltage (Figs. 3b and 6), which is of course a composite quantity with many contributors that make it hard to predict in an absolute sense. (The small nonlinear effect on the current is also readily hidden in assumptions about the mobility, as this too is a poorly known and hard-to-predict quantity). This logic is also the reason why it would be difficult to demonstrate experimentally that the nonlinear corrections are indeed needed. Alternatively, one could say that if a meaningful comparison could be made between theoretical and experimental threshold voltages, then it could be turned around and used to measure some of the nonlinear material coefficients. In any event, it is worth noting that the nonlinear predictions in Figs. 3b and 6 are if anything in closer correspondence with HEMT measurement than are the linear results [36]. It is also possible that the values of coefficients used in linear theory simulations — for example, of $\phi_m - \Delta E_C$, the spontaneous polarizations, and/or the linear piezoelectric coefficients — have been chosen (incorrectly) so as to compensate for the neglect of the nonlinear contributions, an idea that has been suggested previously with respect to nonlinear piezoelectricity [16], [17]. If so, then when applied to more general device situations the incorrectness of the "effective" linear theory could well result in errors whose significance would need to be assessed.

(*ii*) *GaN reliability:* The main application of our previous work using the linear theory of semiconductor thermoelectroelasticity was in the area of GaN HEMT reliability [6]. The specific motivation was observations by various researchers [37], [38] that accelerated temperature-bias stress testing of conventional AlGaN/GaN RF devices often leads to the development of pits and cracks, and especially in the AlGaN layer at the drain side edge of the gate electrode. An intriguing hypothesis proposed to explain this phenomenon was that it might be triggered by piezoelectric

stresses imposed during operation that add to the built-in stresses of the heterostructure and push the AlGaN into failure [37]. The thermoelectroelastic simulations performed in [6] did not, however, support this plausible idea. Instead it was found that the additional piezoelectric stress was not especially large, and indeed was often significantly smaller than the thermal stresses that were present simultaneously due to the device's power dissipation under high-voltage, high-current conditions. Another observation from these simulations was that if an incipient crack developed at the drain end of the gate, then the stress concentration would be such that the crack would quickly propagate across the AlGaN and terminate at the GaN interface with severe effects on the device characteristics [6].

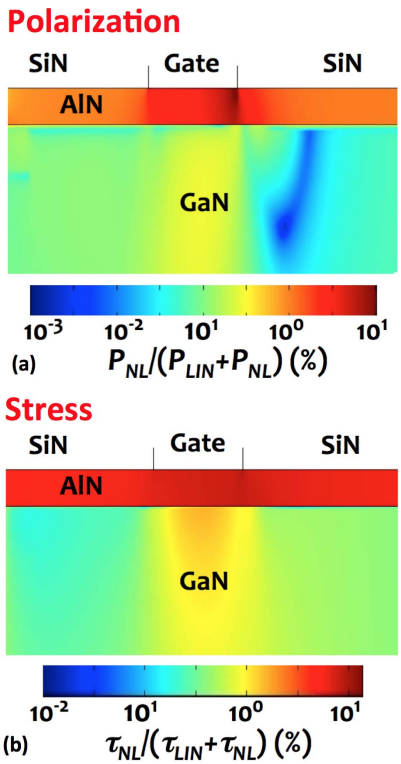

FIGURE 7. Logarithmic field plots of the relative contributions of the nonlinear terms to (a) polarization and (b) stress in an AlGaN/GaN HEMT with $V_D = 20$V. The variations on the left side of these plots arise from the proximity of the source.

Since the stress and strain levels in the HEMTs are very high during accelerated-life-testing, nonlinear effects will undoubtedly be significant, though probably not sufficient to alter the qualitative conclusions reached earlier in [6]. In any event, we explore the situation by first simulating the current-voltage characteristics of an undamaged conventional HEMT biased out to $V_D = 20$ V and comparing results with and without the nonlinear contributions. The I-V result (not shown) is very much like that of Fig. 3a with the nonlinearity reducing the current by just a few percent. Figs. 7a,b are field plots like those of Figs. 5a,b showing the relative size of the polarization and stress nonlinearities. The differences are quite large, *e.g.,* the maximum polarization nonlinearity contribution increases from 2.2% to 74% and the maximum stress nonlinearity contribution increases from 6.2% to 11%.

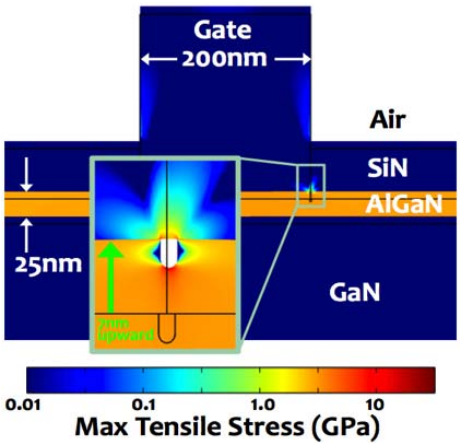

FIGURE 8. Simulated mechanical stresses in a GaN HEMT under high-voltage ON-state biasing ($V_G = 0$ and $V_D = 20$ V) and showing the stress concentration in the vicinity of a small crack situated at the gate edge on the drain side.

As a second set of calculations we examined the situation of a small crack at the drain side edge of the gate and compared simulations performed using the linear and nonlinear theories. A result from the nonlinear simulation is shown in Fig. 8 where we exhibit the principal stress field around the crack. The peak stress at the crack tip is about 12GPa, whereas the same calculation in linear theory puts the stress at about 13GPa. This is an appreciable correction, however given the large uncertainty in the failure strength of the AlGaN (assumed to be roughly 10GPa in [6]), it is hard to say whether it is significant. It is also interesting to note that Fig. 8 shows a slight upward displacement of the transistor by about 7nm due to thermal expansion during operation; we note that measurements of such displacements under much milder conditions by atomic force microscopy have been reported in [39].

(*iii*) *Nanogenerator Device:* A nanogenerator concept was proposed in [40] in which the bending of a cantilever composed of a piezoelectric semiconductor generated polarization charges that caused electrons to flow in/out of contacts. If at least one of these contacts is made rectifying then the design will act as an electron pump that can be used to charge a capacitor or a battery. The intriguing application for this device is that it might be used to harvest electrical energy from incidental mechanical motions, e.g., if the devices were embedded in clothing. In [40] the semiconductor used was ZnO, but analogous devices composed of III-N [41] and other [42] materials have also been investigated. This sub-section discusses the numerical simulation of GaN designs like that depicted schematically in Fig. 9, and for the present paper this example serves as an illustration of the application of the nonlinear theory to semiconducting MEMS devices.

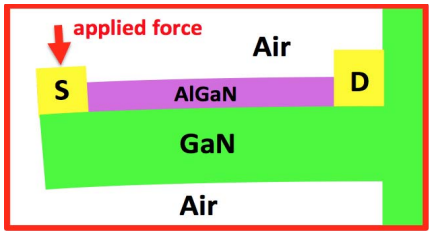

FIGURE 9. Schematic of the AlGaN/GaN nanogenerator in which an applied force produces electrical current flows.

Studies of the mechanics of cantilevers go back to Bernoulli and Euler who considered long thin beams (referred to as *elastica*) in which the bending is elastic with the interesting combination of large displacements/rotations but small strains, with the latter circumstance obviously greatly simplifying the elasticity analysis. Our situation is obviously more complicated since it involves a cantilever composed of a strained layer heterostructure (see Fig. 9) in which there are large built-in strains. In any event, because our approach is entirely numerical there is no need to exploit an approximation in which any component of the strain is small and so no such assumption is made. We assume the nanogenerator cantilever is of infinite width in order to allow a two-dimensional plane-strain treatment. A similar treatment using a two-dimensional plane-stress assumption would model a narrow cantilever and probably better corresponds to most experiments, but this type of analysis is not pursued here. To apply the mechanical force to bend the cantilever, we exert a point load at the free end as might be applied by an AFM tip, however we allow either sign so that the load can pull up as well as push down. The cantilever design has ohmic contacts at both ends so charge can flow in and out as needed to maintain charge neutrality. As noted earlier, a practical design would include a rectifying contact, but this is not done here as it is irrelevant to the dynamics. Also, from the point-of-view of applications the power output will rise with frequency and so one would want to cycle the cantilever as rapidly as possible, but this too is immaterial from our perspective.

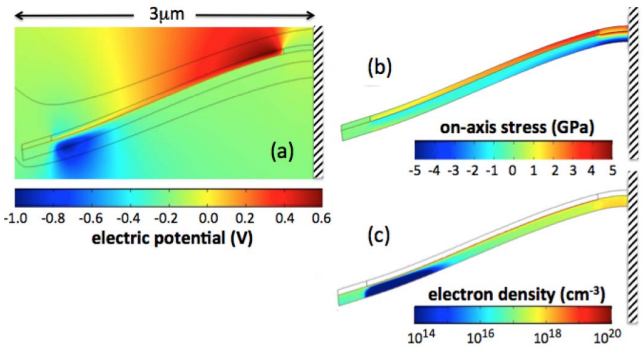

FIGURE 10. Snapshots of (a) electric potential, (b) on-axis stress, and (c) electron density at the lowest point in cyclic motion of GaN nanogenerator.

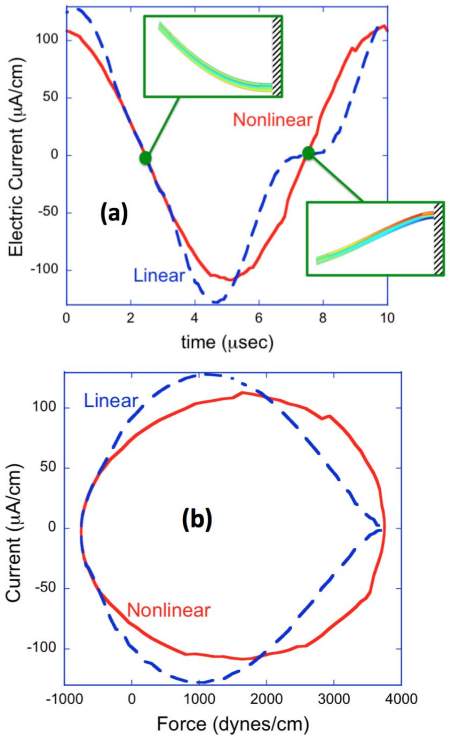

FIGURE 11. (a) The electric current per unit width generated by cantilever versus time as computed using nonlinear and linear theories. The insets show cantilever positions and on-axis stresses at two positions in the cycle. (b) Generated electric current versus applied force (per unit width). Range of validity of linear theory is evident in both plots.

A simulation of a full cycle of the cantilever is readily carried out, and some sample snapshots of the fields inside the device are shown in Figs. 10a-c. The electric potential shows dramatic swings that arise from the changing polarization charge, and it is these electrostatic shifts that result in the desired current flows. The induced nanogenerator current (per unit width) at a contact is plotted in Fig. 11a as a function of time with the prediction of nonlinear theory compared with that of linear theory. The period is 10μsec so the frequency in this case is 100kHz. The insets indicate the cantilever positions (and on-axis stresses) at two points in the cycle. The comparison of the nonlinear and linear results shows the significant size of the nonlinear corrections and the range of validity of the linear approximation with the two simulations agreeing over some range but not beyond. That the linear theory works best under conditions of maximum upward bending is due to the fact that in this condition there is the greatest degree of cancellation of the built-in strains by the flexural strains. Fig. 11b is complementary to Fig. 11a and shows the generated current over a full cycle as a function of the applied force (per unit width). Again results of both nonlinear and linear calculations are shown and the errors made by the latter are apparent.

V. FINAL REMARKS

We have presented a nonlinear theory capable of describing electron and hole transport in piezoelectric semiconductors

under conditions of large mechanical strains/displacements for which the usual assumptions of linearity are not justified. Both kinematic and constitutive nonlinearities are considered with the imposition of rotational invariance being of critical importance. Also receiving careful consideration is the treatment of the electrostatic boundary conditions at free surfaces that are undergoing finite deformation. Numerical simulations of various III-N devices of technological interest are used to illustrate the theory, and these included conventional HEMTs under normal and accelerated-life-testing conditions and semiconducting microelectromechanical structures. Although the values of the various material coefficients are uncertain, the nonlinear corrections are often large and are surely non-negligible. In the case of conventional HEMTs the primary effect is on threshold voltage, and given the uncertainties in this quantity, it would not be surprising if errors here were just never noticed. In the case of the MEMS device, the critical need for the nonlinear theory comes from the need to treat properly large rotations of the structure.

The technological importance of the III-N materials for RF, power, and light-emitting devices is obvious, and applications in these areas is sure to grow in the coming years. With this will come the continued need for engineering-oriented modeling tools that are well-suited to design and optimization, and the methods described in this paper represent a contribution toward this effort. This could occur in the traditional way through their implementation in standard device modeling packages such as those from Synopsys or Silvaco, or alternatively, with the spread of powerful codes like COMSOL [32], implementation within a more general computational framework is becoming increasingly attractive.

APPENDIX
COEFFICIENTS FOR HEXAGONAL III-N MATERIALS

The III-N materials we consider are hexagonal crystals that belong to the *6mm* point group. The symmetries of this group impose restrictions on the material coefficients in the various tensors employed in this paper and these constraints greatly reduce the number of independent coefficients. These matters are discussed in [30] and the forms of the various tensors in a coordinate system where the 3-direction points along the c-axis are as given below with K and L varying from 1 to 3, and A and B varying from 1 to 6 in the usual shorthand for tensor indices of $A \leftrightarrow KL$ with $1 \leftrightarrow 11$, $2 \leftrightarrow 22$, $3 \leftrightarrow 33$, $4 \leftrightarrow 23/32$, $5 \leftrightarrow 13/31$, and $6 \leftrightarrow 12/21$.

$$\{\alpha_{KL}\} = \begin{bmatrix} \alpha_{11} & 0 & 0 \\ 0 & \alpha_{11} & 0 \\ 0 & 0 & \alpha_{33} \end{bmatrix}$$

$$\{\chi_{KL}\} = \begin{bmatrix} \chi_{11} & 0 & 0 \\ 0 & \chi_{11} & 0 \\ 0 & 0 & \chi_{33} \end{bmatrix} \tag{A1}$$

$$\{e_{KA}\} = \begin{bmatrix} 0 & 0 & 0 & 0 & e_{15} & 0 \\ 0 & 0 & 0 & e_{15} & 0 & 0 \\ e_{31} & e_{31} & e_{33} & 0 & 0 & 0 \end{bmatrix} \tag{A2a}$$

$$\{\chi_{KA}\} = \begin{bmatrix} 0 & 0 & 0 & 0 & \chi_{15} & 0 \\ 0 & 0 & 0 & \chi_{15} & 0 & 0 \\ \chi_{31} & \chi_{31} & \chi_{33} & 0 & 0 & 0 \end{bmatrix} \tag{A2b}$$

$$\{C_{AB}\} = \begin{bmatrix} C_{11} & C_{12} & C_{13} & & & \\ C_{12} & C_{11} & C_{13} & & 0 & \\ C_{13} & C_{13} & C_{33} & & & \\ & & & C_{44} & 0 & 0 \\ & 0 & & 0 & C_{44} & 0 \\ & & & 0 & 0 & (C_{11}-C_{12})/2 \end{bmatrix} \tag{A3}$$

$$\{b_{AB}\} = \begin{bmatrix} b_{11} & b_{12} & b_{13} & & & \\ b_{12} & b_{11} & b_{13} & & 0 & \\ b_{31} & b_{31} & b_{33} & & & \\ & & & b_{44} & 0 & 0 \\ & 0 & & 0 & b_{44} & 0 \\ & & & 0 & 0 & (b_{11}-b_{12})/2 \end{bmatrix} \tag{A4}$$

$$\{k_{1AB}\} = \begin{bmatrix} & & & 0 & k_{115} & 0 \\ & 0 & & 0 & k_{125} & 0 \\ & & & 0 & k_{135} & 0 \\ 0 & 0 & 0 & 0 & 0 & k_{146} \\ k_{115} & k_{125} & k_{135} & 0 & 0 & 0 \\ 0 & 0 & 0 & k_{146} & 0 & 0 \end{bmatrix} \tag{A5a}$$

$$k_{146} = (k_{115} - k_{125})\ /2$$

$$\{k_{2AB}\} = \begin{bmatrix} & & & k_{125} & 0 & 0 \\ & 0 & & k_{115} & 0 & 0 \\ & & & k_{135} & 0 & 0 \\ k_{125} & k_{115} & k_{135} & 0 & 0 & 0 \\ 0 & 0 & 0 & 0 & 0 & k_{146} \\ 0 & 0 & 0 & 0 & k_{146} & 0 \end{bmatrix} \tag{A5b}$$

$$\{k_{3AB}\} = \begin{bmatrix} k_{311} & k_{312} & k_{313} & & & \\ k_{312} & k_{311} & k_{313} & & 0 & \\ k_{313} & k_{313} & k_{333} & & & \\ & & & k_{344} & 0 & 0 \\ & 0 & & 0 & k_{344} & 0 \\ & & & 0 & 0 & k_{366} \end{bmatrix} \tag{A5c}$$

$$k_{366} = (k_{311} - k_{312})/2$$

$$\{c_{1AB}\} = \begin{bmatrix} c_{111} & c_{112} & c_{113} & & & \\ c_{112} & c_{122} & c_{123} & & 0 & \\ c_{113} & c_{123} & c_{133} & & & \\ & & & c_{144} & 0 & 0 \\ & 0 & & 0 & c_{155} & 0 \\ & & & 0 & 0 & c_{166} \end{bmatrix} \tag{A6a}$$

$$\{c_{2AB}\} = \begin{bmatrix} c_{112} & c_{122} & c_{123} & & & \\ c_{122} & c_{222} & c_{113} & & 0 & \\ c_{123} & c_{113} & c_{133} & & & \\ & & & c_{155} & 0 & 0 \\ & 0 & & 0 & c_{144} & 0 \\ & & & 0 & 0 & c_{266} \end{bmatrix} \tag{A6b}$$

$$\{c_{3AB}\} = \begin{bmatrix} c_{113} & c_{123} & c_{133} & & & \\ c_{123} & c_{113} & c_{113} & & 0 & \\ c_{133} & c_{133} & c_{333} & & & \\ & & & c_{344} & 0 & 0 \\ & 0 & & 0 & c_{344} & 0 \\ & & & 0 & 0 & c_{366} \end{bmatrix} \quad \text{(A6c)}$$

$$\{c_{4AB}\} = \begin{bmatrix} & & & c_{144} & 0 & 0 \\ & 0 & & c_{155} & 0 & 0 \\ & & & c_{344} & 0 & 0 \\ c_{144} & c_{155} & c_{344} & 0 & 0 & 0 \\ 0 & 0 & 0 & 0 & 0 & c_{456} \\ 0 & 0 & 0 & 0 & c_{456} & 0 \end{bmatrix} \quad \text{(A6d)}$$

$$\{c_{5AB}\} = \begin{bmatrix} & & & 0 & c_{155} & 0 \\ & 0 & & 0 & c_{144} & 0 \\ & & & 0 & c_{344} & 0 \\ 0 & 0 & 0 & 0 & 0 & c_{456} \\ c_{155} & c_{144} & c_{344} & 0 & 0 & 0 \\ 0 & 0 & 0 & c_{456} & 0 & 0 \end{bmatrix} \quad \text{(A6e)}$$

$$\{c_{6AB}\} = \begin{bmatrix} & & & 0 & 0 & c_{166} \\ & 0 & & 0 & 0 & c_{266} \\ & & & 0 & 0 & c_{366} \\ 0 & 0 & 0 & 0 & c_{456} & 0 \\ 0 & 0 & 0 & c_{456} & 0 & 0 \\ c_{166} & c_{266} & c_{366} & 0 & 0 & 0 \end{bmatrix} \quad \text{(A6f)}$$

$$c_{122} = c_{111} + c_{112} - c_{222},\ c_{166} = \frac{1}{4}\left(3c_{222} - 2c_{111} - c_{112}\right)$$

$$c_{266} = \frac{1}{4}\left(2c_{111} - c_{112} - c_{222}\right)$$

$$c_{366} = \frac{1}{2}\left(c_{113} - c_{123}\right),\ c_{456} = \frac{1}{2}\left(c_{155} - c_{144}\right) \quad \text{(A6g)}$$

ACKNOWLEDGMENT

This paper was motivated by collaborations with K. Hobart, D. Meyer, F. Kub, B. Downey, T. Anderson, M. Tadjer, J. Calame, and C. Eddy, all of the Naval Research Laboratory, and their long-term support and interest are much appreciated. Additionally, the author wishes to remember his thesis advisor, the late Prof. Harry F. Tiersten of Rensselaer Polytechnic Institute, for long-ago lessons that made this work possible. Funding from the Office of Naval Research is also gratefully acknowledged.

REFERENCES

[1] A. R. Hutson and D. L. White, "Elastic wave propagation in piezoelectric semiconductors," *J. Appl. Phys.*, vol. 33, no. 1, p. 40, 1962.
[2] M. Rais-Zadeh *et al.*, "Gallium nitride as an electromechanical material," *IEEE J. Microelectromech. Syst.*, vol. 23, no. 6, pp. 1252–1271, Dec. 2014.
[3] Y. Liu, Y. Zhang, Q. Yang, S. Niu, and Z. L. Wang, "Fundamental theories of piezotronics and piezo-phototronics," *Nano Energy*, vol. 14, pp. 257–275, May 2015.
[4] X. Wen *et al.*, "Development and progress in piezotronics," *Nano Energy*, vol. 14, pp. 276–295, May 2015.
[5] B. Jogai, J. D. Albrecht, and E. Pan, "Effect of electromechanical coupling on the strain in AlGaN/GaN heterojunction field effect transistors," *J. Appl. Phys.*, vol. 94, no. 6, p. 3984, 2003.
[6] M. G. Ancona, S. C. Binari, and D. J. Meyer, "Fully coupled thermoelectromechanical analysis of GaN HEMT degradation," *J. Appl. Phys.*, vol. 111, no. 7, Apr. 2012, Art. no. 074504.
[7] M. A. Migliorato *et al.*, "A review of non linear piezoelectricity in semiconductors," *AIP Conf. Proc.*, vol. 1590, no. 1, p. 32, 2014.
[8] C. A. Truesdell and R. A. Toupin, "The classical field theories," in *Encyclopedia of Physics*, vol. 3, S. Flugge, ed. Heidelberg, Germany: Springer-Verlag, 1960.
[9] A. E. Green and J. E. Adkins, *Large Elastic Deformations and Nonlinear Continuum Mechanics*. London, U.K.: Oxford Univ. Press, 1960.
[10] R. A. Toupin, "The elastic dielectric," *J. Rational Mech. Anal.*, vol. 5, no. 6, pp. 849–915, 1956.
[11] H. G. de Lorenzi and H. F. Tiersten, "On the interaction of the electromagnetic field with heat conducting deformable semiconductors," *J. Math. Phys.*, vol. 16, no. 4, p. 938, 1975.
[12] H. F. Tiersten, "On the nonlinear equations of thermoelectroelasticity," *Int. J. Eng. Sci.*, vol. 9, no. 7, p. 587, 1971.
[13] H. F. Tiersten, "On the accurate description of piezoelectric resonators subject to biasing deformations," *Int. J. Eng. Sci.*, vol. 33, no. 15, pp. 2239–2259, 1995.
[14] F. Bernardini, V. Fiorentini, and D. Vanderbilt, "Spontaneous polarization and piezoelectric constants of III-V nitrides," *Phys. Rev. B, Condens. Matter*, vol. 56, no. 16, pp. R10024–R10027, 1997.
[15] M. Feneberg and K. Thonke, "Polarization fields of III-nitrides grown in different crystal orientations," *J. Phys. Condens. Matter*, vol. 19, no. 40, 2007, Art. no. 403201.
[16] J. Pal, G. Tse, V. Haxha, M. A. Migliorato, and S. Tomic, "Second-order piezoelectricity in wurtzite III-N semiconductors," *Phys. Rev. B, Condens. Matter*, vol. 84, no. 8, Aug. 2011, Art. no. 085211.
[17] M. A. Migliorato *et al.*, "A review of non linear piezoelectricity in semiconductors," *AIP Conf. Proc.*, vol. 1590, no. 1, p. 32, 2014.
[18] C. E. Dreyer, A. Janotti, C. G. Van de Walle, and D. Vanderbilt, "Correct implementation of polarization constants in wurtzite materials and impact on III-nitrides," *Phys. Rev. X*, vol. 6, no. 2, 2016, Art. no. 021038.
[19] I. L. Guy, S. Muensit, and E. M. Goldys, "Electrostriction in gallium nitride," *Appl. Phys. Lett.*, vol. 75, no. 23, p. 3641, 1999.
[20] R. Clos, A. Dadgar, and A. Krost, "Wafer curvature in the nonlinear deformation range," *Phys. Status Solidi A*, vol. 201, no. 11, pp. R75–R78, 2004.
[21] L. Pedesseau, C. Katan, and J. Even, "On the entanglement of electrostriction and non-linear piezoelectricity in non-centrosymmetric materials," *Appl. Phys. Lett.*, vol. 100, no. 3, 2012, Art. no. 031903.
[22] S. N. Rashkeev, W. R. L. Lambrecht, and B. Segall, "Efficient *ab initio* method for the calculation of frequency-dependent second-order optical response in semiconductors," *Phys. Rev. B, Condens. Matter*, vol. 57, no. 7, pp. 3905–3919, 1998.
[23] M. Lopuszynski and J. Majewski, "*Ab initio* calculations of third-order elastic constants and related properties for elected semiconductors," *Phys. Rev. B, Condens. Matter*, vol. 76, no. 4, Jul. 2007, Art. no. 045202.
[24] Y. Cho and K. Yamanouchi, "Nonlinear, elastic, piezoelectric, electrostrictive, and dielectric constants of lithium niobate," *J. Appl. Phys.*, vol. 61, no. 3, p. 875, Feb. 1987.
[25] A. E. Green and R. S. Rivlin, "Simple force and stress multipoles," *Archive Rational Mech. Anal.*, vol. 16, no. 5, pp. 325–353, 1964.
[26] M. G. Ancona, "Hydrodynamic models of semiconductor electron transport at high fields," *VLSI Design*, vol. 3, no. 2, pp. 101–114, 1995.
[27] B. P. Downey *et al.*, "Effect of SiN_x gate insulator thickness on electrical properties of SiN_x/$In_{0.17}Al_{0.83}N$/AlN/GaN MIS–HEMTs," *Solid State Electron.*, vol. 106, pp. 12–17, Apr. 2015.
[28] W. Adam, J. Tichy, and E. Kittinger, "The different sets of electrical, mechanical, and electromechanical third-order constants for quartz," *J. Appl. Phys.*, vol. 64, no. 5, pp. 2556–2562, 1988.
[29] H. W. Then *et al.*, "High-K gate dielectric depletion-mode and enhancement-mode GaN MOS-HEMTs for improved OFF-state leakage and DIBL for power electronics and RF applications," in *Proc. IEDM*, 2015, pp. 418–421.
[30] D. F. Nelson, *Electric, Optic, and Acoustic Interactions in Dielectrics*. New York, NY, USA: Wiley, 1979.
[31] S. Selberherr, *Analysis and Simulation of Semiconductor Devices*. New York, NY, USA: Springer-Verlag, 1984.

[32] *Comsol Inc.* Accessed on Jul. 29, 2017. [Online]. Available: http://www.comsol.com
[33] J. Donea, A. Huerta, J.-P. Ponthot, and A. Rodriguez-Ferran, "Arbitrary Lagrangian–Eulerian methods," in *Encyclopedia of Computational Mechanics*, vol. 1, E. Stein, R. de Boor, and T. Hughes, Eds. New York, NY, USA: Wiley, 2004, ch. 14.
[34] O. Ambacher *et al.*, "Two dimensional electron gases induced by spontaneous and piezoelectric polarization in undoped and doped AlGaN/GaN heterostructures," *J. Appl. Phys.*, vol. 87, no. 1, p. 334, 2000.
[35] Y. Cao and D. Jena, "High-mobility window for two-dimensional electron gases at ultrathin AlN/GaN heterojunctions," *Appl. Phys. Lett.*, vol. 90, no. 18, 2007, Art. no. 182112.
[36] S. C. Binari *et al.*, "Trapping effects and microwave power performance in AlGaN/GaN HEMTs," *IEEE Trans. Electron Devices*, vol. 48, no. 3, pp. 465–471, Mar. 2001.
[37] U. Chowdhury *et al.*, "TEM observation of crack- and pit-shaped defects in electrically degraded GaN HEMTs," *IEEE Electron Device Lett.*, vol. 29, no. 10, pp. 1098–1100, Oct. 2008.
[38] P. Makaram, J. Joh, J. A. del Alamo, T. Palacios, and C. V. Thompson, "Evolution of structural defects associated with electrical degradation in AlGaN/GaN high electron mobility transistors," *Appl. Phys. Lett.*, vol. 96, no. 23, 2010, Art. no. 233509.
[39] M. R. Rosenberger, J. P. Jones, E. R. Heller, S. Graham, and W. P. King, "Nanometer-scale strain measurements in AlGaN/GaN high-electron mobility transistors during pulsed operation," *IEEE Trans. Electron Devices*, vol. 63, no. 7, pp. 2742–2748, Jul. 2016.
[40] Z. L. Wang and J. Song, "Piezoelectric nanogenerators based on zinc oxide nanowire arrays," *Science*, vol. 312, no. 5771, pp. 242–246, Apr. 2006.
[41] X. Wang *et al.*, "Electricity generation based on one-dimensional group-III nitride nanomaterials," *Adv. Mater.*, vol. 22, no. 19, pp. 2155–2158, 2010.
[42] S. S. Won *et al.*, "Piezoelectric poly(vinylidene fluoride trifluoroethylene) thin film-based power generators using paper substrates for wearable device applications," *Appl. Phys. Lett.*, vol. 107, no. 20, 2015, Art. no. 202901.

M. G. ANCONA (M'79) has been a Staff Member with the Electronics Science and Engineering Division, Naval Research Laboratory for 33 years, where he has researched in many areas of semiconductor device physics, modeling, and engineering. He also taught part-time for 18 years with the Johns Hopkins University. He has authored a book entitled *Computational Methods for Applied Science and Engineering* (Rinton Press, Princeton, 2002, p. 606).